Controlled Supramolecular Self-Assembly of Large Nanoparticles in Amphiphilic Brush Block Copolymers

Dong-Po Song,[†] Ying Lin,[†] Yue Gai,[†] Nicholas S. Colella,[†] Cheng Li,[†] Xiao-Hui Liu,[†] Samuel Gido,[†] and James J. Watkins*,[†]

[†]Department of Polymer Science and Engineering, University of Massachusetts Amherst, 120 Governors Drive, Amherst, Massachusetts 01003, United States

S *Supporting Information*

ABSTRACT: To date the self-assembly of ordered metal nanoparticle (NP)/block copolymer hybrid materials has been limited to NPs with core diameters (D_{core}) of less than 10 nm, which represents only a very small fraction of NPs with attractive size-dependent physical properties. Here this limitation has been circumvented using amphiphilic brush block copolymers as templates for the self-assembly of ordered, periodic hybrid materials containing large NPs beyond 10 nm. Gold NPs (D_{core} = 15.8 ± 1.3 nm) bearing poly(4-vinylphenol) ligands were selectively incorporated within the hydrophilic domains of a phase-separated (polynorbornene-*g*-polystyrene)-*b*-(polynorbornene-*g*-poly(ethylene oxide)) copolymer via hydrogen bonding between the phenol groups on gold and the PEO side chains of the brush block copolymer. Well-ordered NP arrays with an inverse cylindrical morphology were readily generated through an NP-driven order−order transition of the brush block copolymer.

Metal nanoparticles (NPs) with core diameters (D_{core}) of a few to tens of nanometers have been widely investigated in a variety of fields, including the life sciences, light and energy management, electronics, and environmental sciences, because of their unique size-dependent physical properties.[1] The most attractive size range for a particular NP core often depends on its intended purpose, e.g., achieving a desired emission wavelength for a quantum dot or exploiting a localized surface plasmon resonance (LSPR) in noble-metal NPs. Precise control over their spatial organization on different length scales is central to improve the performance of next-generation materials and devices, ranging from sensors and memory storage devices to photovoltaic, nonlinear optical, plasmonic, and other electronic nanodevices.[2]

Linear block copolymers (BCPs) can self-assemble into periodic spherical, cylindrical, bicontinuous, and lamellar morphologies, and they play an important role in directing the self-assembly of small NPs with core diameters of a few nanometers.[3] The accommodation and distribution of NPs in linear BCPs greatly depend on a delicate balance of the enthalpic contributions arising from the interactions between NP ligands and BCP segments and the entropic loss due to polymer chain stretching for incorporation of NPs.[4−13] Chemical modification of NP surface properties, for example, has proven to be an effective approach to sequester NPs within certain domains of BCP templates by introducing neutral or favorable interactions between the surface ligands and specific blocks, such as van der Waals interactions,[5,6] hydrogen bonding,[9,10] or ionic interactions.[11] Strong favorable interactions between NPs and the host BCP can offset the entropic penalty associated with their addition, enabling high NP loadings and avoiding macrophase separation of the NPs.[9]

Despite the great success achieved using linear BCPs to template NP arrays, the self-assembly of large NPs with D_{core} > 10 nm within linear BCP microdomains that are only a few tens of nanometers in width has remained challenging because of both the need to effectively stabilize large NPs against self-aggregation and the significant loss in conformational entropy associated with polymer chain stretching around these large obstacles.[8] In this Communication, we demonstrate a facile strategy for fabrication of well-ordered nanocomposites with high filling fractions (25 vol %) of large NPs (D_{core} > 15 nm). This technique utilizes an amphiphilic brush BCP as the template and hydrogen bonding as the driving force for the selective incorporation of the NPs into hydrophilic domains (see Scheme 1). An order−order transition of the brush BCP

Scheme 1. Illustration of Gold NP Self-Assembly in PS-*b*-PEO Brush BCPs through Hydrogen-Bonding Interactions between Phenol Groups on the Gold Surface and PEO Side Chains of the BCP; A Cylindrical Morphology Is Formed as a Result of an NP-Induced Asymmetry of the Side-Chain Lengths of a Symmetric Brush BCP
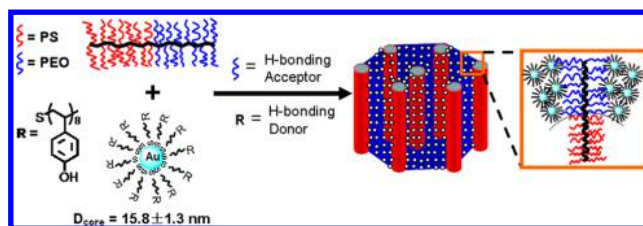

from a lamellar to a cylindrical morphology was observed at high NP loadings. We believe that this is the first such order−order transition observed in brush block copolymers, where cylindrical morphologies in neat brush copolymer systems are attributed to asymmetries in the side-chain lengths.

Recently there has been great success in the design and synthesis of brush BCPs that show substantially reduced polymer chain entanglements relative to their linear analogues. This enables rapid self-assembly to yield nanostructures with domain sizes beyond 100 nm.[14−19] Introducing large NPs into the large microdomains of phase-separated brush BCPs is of great interest to investigate the phase behavior of brush BCPs in the presence of large NPs and fabricate novel nanostructured hybrid materials with greatly expanded domain spacings. In the present work, the brush BCP was a (polynorbornene-g-polystyrene)-b-(polynorbornene-g-poly(ethylene oxide)) copolymer ((PNB−PS$_{3.5k}$)$_{86}$-b-(PNB−PEO$_{2k}$)$_{104}$) (M_n = 487 kg/mol, f_{PEO} ∼ 41 vol %) synthesized by living ring-opening metathesis polymerization (ROMP). The synthesis and characterization of a family of the brush BCPs are described in a separate paper,[20] in which we focus on the optical properties of nanocomposites containing small NPs (D_{core} = 2 nm). The molecular weight of the PS brushes was 3.5 kg/mol (about 33 repeat units), while the PEO brushes had a molecular weight of 2.0 kg/mol (about 45 repeat units). Similar to the reported bottle brush BCPs,[15−19] these PS-b-PEO brush BCPs self-assembled into well-ordered lamellar morphologies in less than 5 min at 130 °C, as indicated by small-angle X-ray scattering (SAXS) profiles (Figure S1 in the Supporting Information).

The gold NPs were initially stabilized by citrate ligands and subsequently coated with thiol-terminated poly(4-vinylphenol) (P4HS) via ligand exchange (see the Supporting Information for detailed information). The molecular weight of the P4HS was around 1.0 kg/mol (about 8 repeat units). As shown in Figure 1, the average core diameter of the gold NPs was
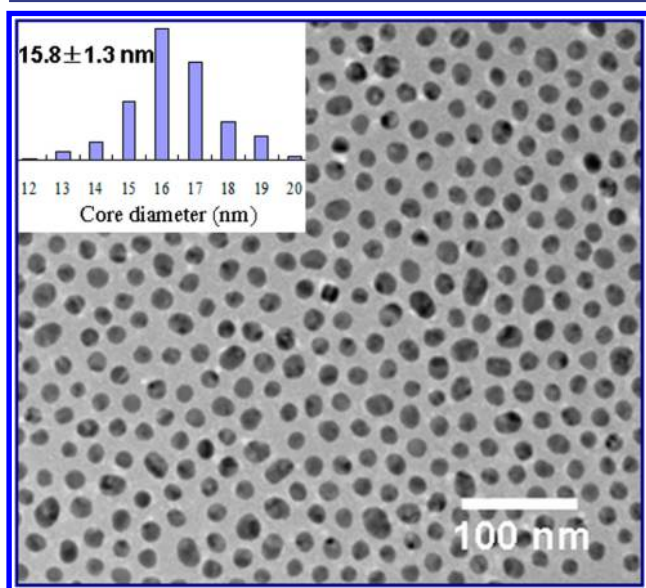

Figure 1. TEM micrograph and (inset) core size distribution of the large gold NPs (D_{core} = 15.8 ± 1.3 nm) coated with poly(4-vinylphenol) ligands (M_n = 1.0 kg/mol, PDI = 1.1).

approximately 15.8 nm on the basis of an analysis of the transmission electron microscopy (TEM) micrograph using ImageJ software. Thermogravimetric analysis (TGA) indicated that the gold core represented 68 wt % of the gold NPs (Figure S2). The ligands are not only effective stabilizers for the large gold NPs in solution but also act as hydrogen-bond donors that

exhibit strong interactions with the PEO side chains of the brush BCPs in the nanocomposites.

For the brush BCP−NP composites, we typically prepared 2% (w/v) polymer solutions in anhydrous dimethylformamide (DMF) admixed with various amounts of the gold NPs, resulting in different weight percentages in the solid. Herein the weight percentage of NPs in the composites is based on the mass of the NP core and ligand shell, while the volume percentage of NPs (core + ligand) can be estimated using the TGA data and the densities of the components and is provided in parentheses following the first mention of the NP weight percentage for each composite (see details in the Supporting Information). The composite films were prepared simply by drop-casting the mixture solutions on horizontal silicon substrates. After solvent evaporation, the dried films were further annealed in saturated dichloromethane (DCM) vapor at room temperature for 3 days. The morphologies of the brush BCP−NP composites were determined by TEM and field-emission scanning electron microscopy (FESEM). Samples for TEM were prepared by cryogenic microtoming of epoxy-supported bulk films and, in some cases, by subsequent selective staining of the PEO domains using RuO$_4$. Samples for cross-sectional FESEM were prepared by cryofracture of the bulk samples.

Figure 2 shows TEM micrographs of the PS-b-PEO brush BCP and the nanocomposites containing the large gold NPs at
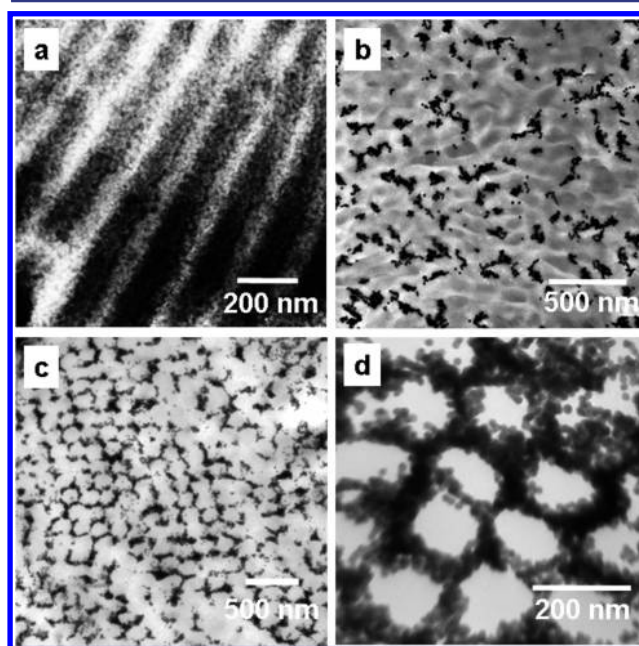


Figure 2. (a) TEM micrograph of the brush BCP (PNB−PS$_{3.5k}$)$_{86}$-b-(PNB−PEO$_{2k}$)$_{104}$ (M_n = 487 kg/mol, f_{PEO} ∼ 41 vol %), showing a well-ordered lamellar morphology. The sample was stained with RuO$_4$ vapor. (b−d) Unstained TEM micrographs of blends of the brush BCP with various loadings of large gold NPs: (b) 15 wt % (5.5 vol %); (c) 30 wt % (12 vol %); (d) 50 wt % (25 vol %).

different loading percentages ranging from 15 wt % (5.5 vol %) to 50 wt % (25 vol %). Figure 2a reveals a highly ordered lamellar morphology of the phase-separated neat polymer with the stained PEO domains appearing as the darker regions, consistent with the SAXS data (Figure S1). Interestingly, a morphology transition from the ordered lamellae to a disordered state (Figure 2b) was observed for the composite

sample containing 5.5 vol % gold NPs. Further increasing the loading percentage to 12 vol % resulted in a cylindrical morphology with PS domains as the cylinders and PEO domains containing the gold NPs as the matrix (Figure 2c). The cylindrical morphology was also produced in the sample containing a higher concentration (25 vol %) of the gold NPs (Figure 2d). Moreover, Figures S3 and S4 show TEM micrographs of an ultramicrotomed bulk sample recorded at the regions with parallel and a certain angle of orientation relative to the cylindrical domain axis.

Because of the large amounts of metal NPs selectively incorporated within the PEO domains and the wide lattice spacing, cross-sectional imaging of the composite sample was possible without staining using FESEM operating at a low voltage and a low beam current. Figure 3 shows FESEM
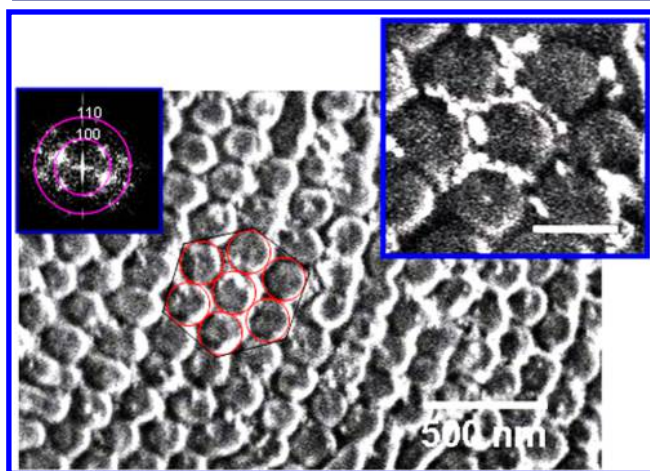
Figure 3. Cross-sectional FESEM micrographs of the nanocomposites containing 12 vol % gold NPs with a Fourier transform, showing a hexagonal lattice with an average domain spacing of 181 nm. The scale bar in the inset FESEM image corresponds to 200 nm.

micrographs of the nanocomposites containing 12 vol % gold NPs, corresponding to Figure 2c, and a Fourier transform of the image suggests a hexagonal lattice. The average domain spacing of the hexagonal lattice was approximately 181 nm as measured using ImageJ. In the inset FESEM image, gold NP clusters can be clearly identified as the white regions in the PEO matrix, which is consistent with the TEM results. A FESEM micrograph showing a larger area of the cryofractured surface of the bulk sample can be found in Figure S5.

There are two possible reasons for the formation of a cylindrical morphology from the self-assembly of the brush BCP: the difference in volume fractions (f_{PS} vs $f_{(PEO+NP)}$) and the asymmetry of the side-chain lengths (l_{PS} vs $l_{(PEO+NP)}$). For the nanocomposites containing 12 vol % NPs (Figures 2c and 3), an order−order transition occurred at a total volume fraction of PEO and NPs ($f_{(PEO+NP)}$) of 47 vol %. This is significantly different from the nanocomposites based on linear BCPs, e.g., PS-b-P2VP, which usually require a much higher concentration of NPs ($f_{(P2VP+NP)} > 65$ vol %) to induce a morphology transition.[21] A recent simulation result showed that the molecular asymmetry required for the formation of cylindrical domains from the self-assembly of a brush BCP is not introduced by the difference in volume fractions but rather by the asymmetry in the side-chain lengths.[22] This explanation is also supported by other experimental results in which a cylindrical morphology was formed by the self-assembly of

brush BCPs with a difference in side-chain lengths.[17,18] In our case, the apparent asymmetry of the side-chain lengths ($l_{PS} < l_{(PEO+NP)}$) may increase as a result of the formation of a supramolecular complex between the large NP and the PEO side chain (Scheme 1), although the driving force behind order−order transitions in brush BCP−NP hybrids requires additional study.

In summary, we have presented a simple strategy for the fabrication of well-ordered functional nanocomposites containing high loadings of large NPs with core diameters of over 15 nm. The large domain size of the PS-b-PEO brush BCPs greatly enhances their utility as templates for the controlled self-assembly of large NPs. A well-ordered cylindrical morphology in the nanocomposites was observed as a result of NP-induced phase transitions of the brush BCPs. This study not only provides insight into the phase behaviors of brush BCPs but also offers new opportunities for creating functional nanocomposites with greatly expanded lattice parameters and controlled spatial arrangements of large NPs with size-dependent behaviors, which provides a platform for the fabrication of plasmonic, nonlinear optical, energy harvesting, electronic, and memory devices. Further investigations of NP size effects on the morphology of nanocomposites based on the brush BCPs are underway.

■ ASSOCIATED CONTENT

ⓢ Supporting Information

Experimental information, SAXS profiles of the PS-b-PEO brush block copolymers, and TEM and FESEM micrographs of the composite samples. This material is available free of charge via the Internet at http://pubs.acs.org.

■ AUTHOR INFORMATION

Corresponding Author

*watkins@polysci.umass.edu

Notes

The authors declare no competing financial interest.

■ ACKNOWLEDGMENTS

■ REFERENCES

(1) (a) Choi, C. L.; Alivisatos, A. P. *Annu. Rev. Phys. Chem.* **2010**, *61*, 369. (b) Talapin, D. V.; Lee, J.-S.; Kovalenko, M. V.; Shevchenko, E. V. *Chem. Rev.* **2010**, *110*, 389.

(2) (a) Huynh, W. U.; Dittmer, J. J.; Alivisatos, A. P. *Science* **2002**, *295*, 2425. (b) Lopes, W. A.; Jaeger, H. M. *Nature* **2001**, *414*, 735. (c) Park, S.; Lee, D. H.; Xu, J.; Kim, B.; Hong, S. W.; Jeong, U.; Xu, T.; Russell, T. P. *Science* **2009**, *323*, 1030. (d) De Rosa, C.; Auriemma, F.; Di Girolamo, R.; Pepe, G. P.; Napolitano, T.; Scaldaferri, R. *Adv. Mater.* **2010**, *22*, 5414. (e) Xiang, J.; Lu, W.; Hu, Y.; Wu, Y.; Yan, H.; Lieber, C. M. *Nature* **2006**, *441*, 489. (f) Briseno, A. L.; Yang, P. *Nat. Mater.* **2009**, *8*, 7. (g) Rancatore, B. J.; Mauldin, C. E.; Tung, S.-H.; Wang, C.; Hexemer, A.; Strzalka, J.; Fréchet, J. M. J.; Xu, T. *ACS Nano* **2010**, *4*, 2721. (h) Wei, Q. S.; Lin, Y.; Anderson, E. R.; Briseno, A. L.; Gido, S. P.; Watkins, J. J. *ACS Nano* **2012**, *6*, 1188.

(3) See the following reviews and references therein: (a) Orilall, M. C.; Wiesner, U. *Chem. Soc. Rev.* **2011**, *40*, 520. (b) Kao, J.;

Thorkelsson, K.; Bai, P.; Rancatoreb, B. J.; Xu, T. *Chem. Soc. Rev.* **2013**, *42*, 2654.

(4) Lee, J. Y.; Thompson, R. B.; Jasnow, D.; Balazs, A. C. *Phys. Rev. Lett.* **2002**, *89*, No. 155503.

(5) Bockstaller, M. R.; Lapetnikov, Y.; Margel, S.; Thomas, E. L. *J. Am. Chem. Soc.* **2003**, *125*, 5276.

(6) Chiu, J. J.; Kim, B. J.; Kramer, E. J.; Pine, D. J. *J. Am. Chem. Soc.* **2005**, *127*, 5036.

(7) Lin, Y.; Boker, A.; He, J. B.; Sill, K.; Xiang, H. Q.; Abetz, C.; Li, X. F.; Wang, J.; Emrick, T.; Long, S.; Wang, Q.; Balazs, A.; Russell, T. P. *Nature* **2005**, *434*, 55.

(8) Balazs, A. C.; Emrick, T.; Russell, T. P. *Science* **2006**, *314*, 1107.

(9) Lin, Y.; Daga, V. K.; Anderson, E. R.; Gido, S. P.; Watkins, J. J. *J. Am. Chem. Soc.* **2011**, *133*, 6513.

(10) Jang, S. G.; Kramer, E. J.; Hawker, C. J. *J. Am. Chem. Soc.* **2011**, *133*, 16986.

(11) Warren, S. C.; Messina, L. C.; Slaughter, L. S.; Kamperman, M.; Zhou, Q.; Gruner, S. M.; DiSalvo, F. J.; Wiesner, U. *Science* **2008**, *320*, 1748.

(12) Zhao, Y.; Thorkelsson, K.; Mastroianni, A. J.; Schilling, T.; Luther, J. M.; Rancatore, B. J.; Matsunaga, K.; Jinnai, H.; Wu, Y.; Poulsen, D.; Fréchet, J. M. J.; Alivisatos, A. P.; Xu, T. *Nat. Mater.* **2009**, *8*, 979.

(13) Kao, J.; Bai, P.; Lucas, J. M.; Alivisatos, A. P.; Xu, T. *J. Am. Chem. Soc.* **2013**, *135*, 1680.

(14) Xia, Y.; Kornfield, J. A.; Grubbs, R. H. *Macromolecules* **2009**, *42*, 3761.

(15) Xia, Y.; Olsen, B. D.; Kornfield, J. A.; Grubbs, R. H. *J. Am. Chem. Soc.* **2009**, *131*, 18525.

(16) Sveinbjörnsson, B. R.; Weitekamp, R. A.; Miyake, G. M.; Xia, Y.; Atwater, H. A.; Grubbs, R. H. *Proc. Natl. Acad. Sci. U.S.A.* **2012**, *109*, 14332.

(17) Bolton, J.; Rzayev, J. *ACS Macro Lett.* **2012**, *1*, 15.

(18) Bolton, J.; Bailey, T. S.; Rzayev, J. *Nano Lett.* **2011**, *11*, 998.

(19) Gu, W.; Huh, J.; Hong, S. W.; Sveinbjornsson, B. R.; Park, C.; Grubbs, R. H.; Russell, T. P. *ACS Nano* **2013**, *7*, 2551.

(20) Song, D.-P.; Li, C.; Colella, N. S.; Lu, X.; Lee, J.-H.; Watkins, J. J. *Adv. Opt. Mater.* **2015**, submitted for publication.

(21) Jang, S. G.; Khan, A.; Hawker, C. J.; Kramer, E. J. *Macromolecules* **2012**, *45*, 1553.

(22) Chremos, A.; Theodorakis, P. E. *ACS Macro Lett.* **2014**, *3*, 1096.